



Ash generation and distribution from the April–May 2010 eruption of Eyjafjallajökull, Iceland

SUBJECT AREAS:

VOLCANOLOGY

GEOLOGY

GEOPHYSICS

ATMOSPHERIC SCIENCE

Magnús T. Gudmundsson¹, Thorvaldur Thordarson², Ármann Höskuldsson¹, Guðrún Larsen¹, Halldór Björnsson³, Fred J. Prata⁴, Björn Oddsson¹, Eyjólfur Magnússon¹, Thórdís Högnadóttir¹, Guðrún Nína Petersen³, Chris L. Hayward², John A. Stevenson² & Ingibjörg Jónsdóttir¹

Received
19 April 2012

Accepted
30 July 2012

Published
14 August 2012

Correspondence and
requests for materials
should be addressed to
M.T.G. (mtg@hi.is)

¹Nordvulk, Institute of Earth Sciences, University of Iceland, Sturlugata 7, 101 Reykjavík, Iceland, ²Grant Institute, University of Edinburgh, The King's Buildings, West Mains Road, Edinburgh EH9 3JW, UK, ³Icelandic Meteorological Office, Bústadavegi 9, 150 Reykjavík, Iceland, ⁴Climate & Atmosphere Dept., Norwegian Inst. for Air Res., N-2027 Kjeller, Norway.

The 39-day long eruption at the summit of Eyjafjallajökull volcano in April–May 2010 was of modest size but ash was widely dispersed. By combining data from ground surveys and remote sensing we show that the erupted material was $4.8 \pm 1.2 \cdot 10^{11}$ kg (benmoreite and trachyte, dense rock equivalent volume 0.18 ± 0.05 km³). About 20% was lava and water-transported tephra, 80% was airborne tephra (bulk volume 0.27 km³) transported by 3–10 km high plumes. The airborne tephra was mostly fine ash (diameter <1000 µm). At least $7 \cdot 10^{10}$ kg (70 Tg) was very fine ash (<28 µm), several times more than previously estimated via satellite retrievals. About 50% of the tephra fell in Iceland with the remainder carried towards south and east, detected over ~7 million km² in Europe and the North Atlantic. Of order 10^{10} kg (2%) are considered to have been transported longer than 600–700 km with < 10^8 kg (<0.02%) reaching mainland Europe.

Tephra dispersal from explosive eruptions is a function of multiple factors, including magma discharge, degree of magma fragmentation, vent geometry, plume height, particle size distribution, and wind velocity. Plinian eruptions, with typical duration of hours, are characterized by magma discharge of 10^7 – 10^8 kg s⁻¹ supporting 20–45 km high plumes often producing tephra falls covering $\geq 10^6$ km² (ref. 1–2). Such dispersal has hitherto not been anticipated for smaller explosive events. The explosive summit eruption of Eyjafjallajökull in Iceland in 14 April–22 May 2010 was a moderate size event (VEI = 3 based on maximum plume height and magma discharge) typified by pulsating explosive activity. The magma discharge never came close to that of Plinian eruptions, but it had a sustained character and duration of weeks. Its ash dispersal was also greater than previously reported for an event of this magnitude. Plinian and other explosive eruptions in Iceland have repeatedly produced ash plumes transported over thousands of kilometres and the latest pre-2010 event to do so and produce plumes that reached Europe was the 50-min long initial explosive phase of the 1947 Hekla eruption³. However, since the introduction in the 1960s of jet-engine powered passenger aircraft, which are vulnerable to exposure to volcanic ash, plumes from explosive eruptions in Iceland were not dispersed towards Europe until Eyjafjallajökull erupted in 2010.

The combination of a prolonged and sustained eruption of fine ash and persistent northwesterly winds transporting the ash towards southeast, resulted in dispersal of ash over a large part of Europe, even though concentrations were everywhere quite low^{4–7}. The resulting unprecedented disruption to air traffic and the implications for vulnerability of modern society to even relatively modest eruptions, have made Eyjafjallajökull 2010 a landmark event. The detail of distal detection of minor amounts of ash in the atmosphere through the use of various techniques and observations is without precedent, and provide unique data for various ash and atmospheric studies. Hence, accurate definition of the source parameters of this eruption is important to realise the full potential of these various data. The aims of this paper are therefore to report and analyse:

- (1) the main phases of the eruption, their characteristics and the in situ measured magnitude and distribution of volcanic ash;
- (2) the grain sizes observed in the first and most powerful explosive phase of the eruption;
- (3) in-situ measured quantity of fine grained ash and compare with observations of airborne ash concentrations obtained by remote sensing;
- (4) the lessons learned about the ash dispersal from modest explosive eruptions in Iceland.



Results

Eruption overview. When signs of unrest were detected in 1992, the volcano of Eyjafjallajökull had been quiet since the eruption of 1821–23. The pre-2010 unrest was signified by discrete periods of seismic swarms and uplift and culminated in two eruptions in 2010 (ref. 8). Inflation in 1994 and 1999–2000 was interpreted as resulting from intrusions at 6–8 km depth in the crust under the volcano^{8,9}. Intense seismicity and uplift in January–March 2010 (ref. 8) was followed by a small basaltic flank eruption on 20 March–12 April¹⁰, forming a 1.3 km² lava flow field with a volume of 0.020 km³ (Fig. 1). The summit eruption started at ca. 1:30 UTC on 14 April and was preceded by an intense three-hour-long earthquake swarm⁸.

Excluding the brief (3–4 hours) subglacial phase when the eruption melted its way through the 200 m thick glacier in the summit caldera, the eruption can be divided into four distinct phases (Fig. 2). The results on Figure 2 are based on combination of fallout data (Figs. 3, 4 and 5) and models of tephra dispersal outside Iceland (Fig. 6). Magma discharges were obtained from combining information from tephra fallout maps (Figs. 3–5) and plume height variations with time (see Methods):

- I. *Initial/First explosive phase (14–18 April).* This phase was characterised by magma discharge of $5\text{--}10\cdot 10^5 \text{ kg s}^{-1}$ ($\approx 200\text{--}400 \text{ m}^3 \text{ s}^{-1}$ DRE) from a water-filled vent, supporting

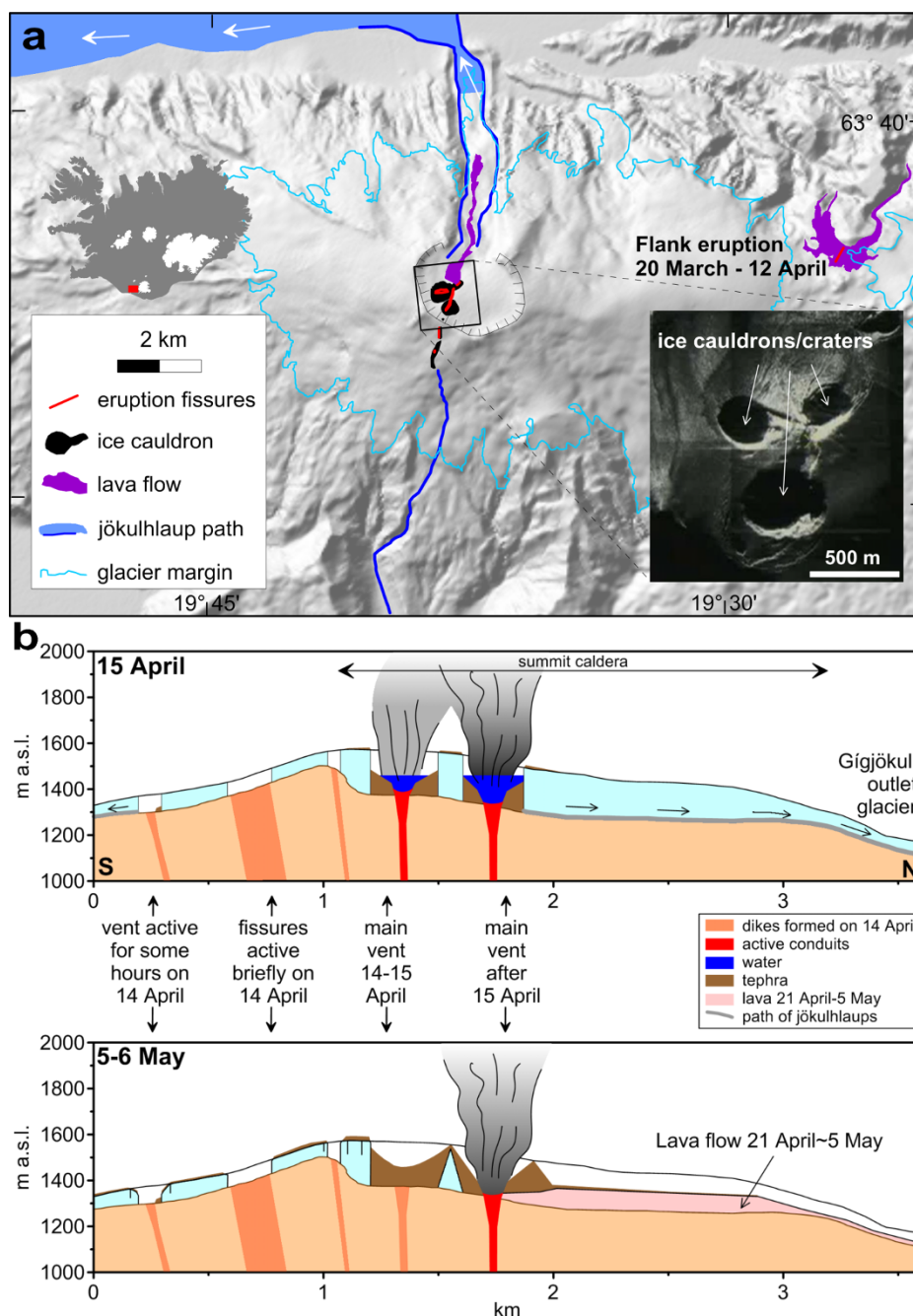


Figure 1 | Setting of the Eyjafjallajökull eruption. (a) The eruption sites, ice cauldrons and pathways of jökulhlaups (glacial floods). Inset on right: an airborne synthetic aperture radar image from 15 April. Inset on left: Iceland and location of Eyjafjallajökull. (b) A north-south cross-section through the main craters within the summit caldera showing the two main ice cauldrons with the vents (south cauldron active 14–15 April and west cauldron active from 15 April) and pathways of meltwater on 15 April (upper panel) and 5–6 May (lower panel). The location and form of subsurface volcanic conduits is highly schematic.

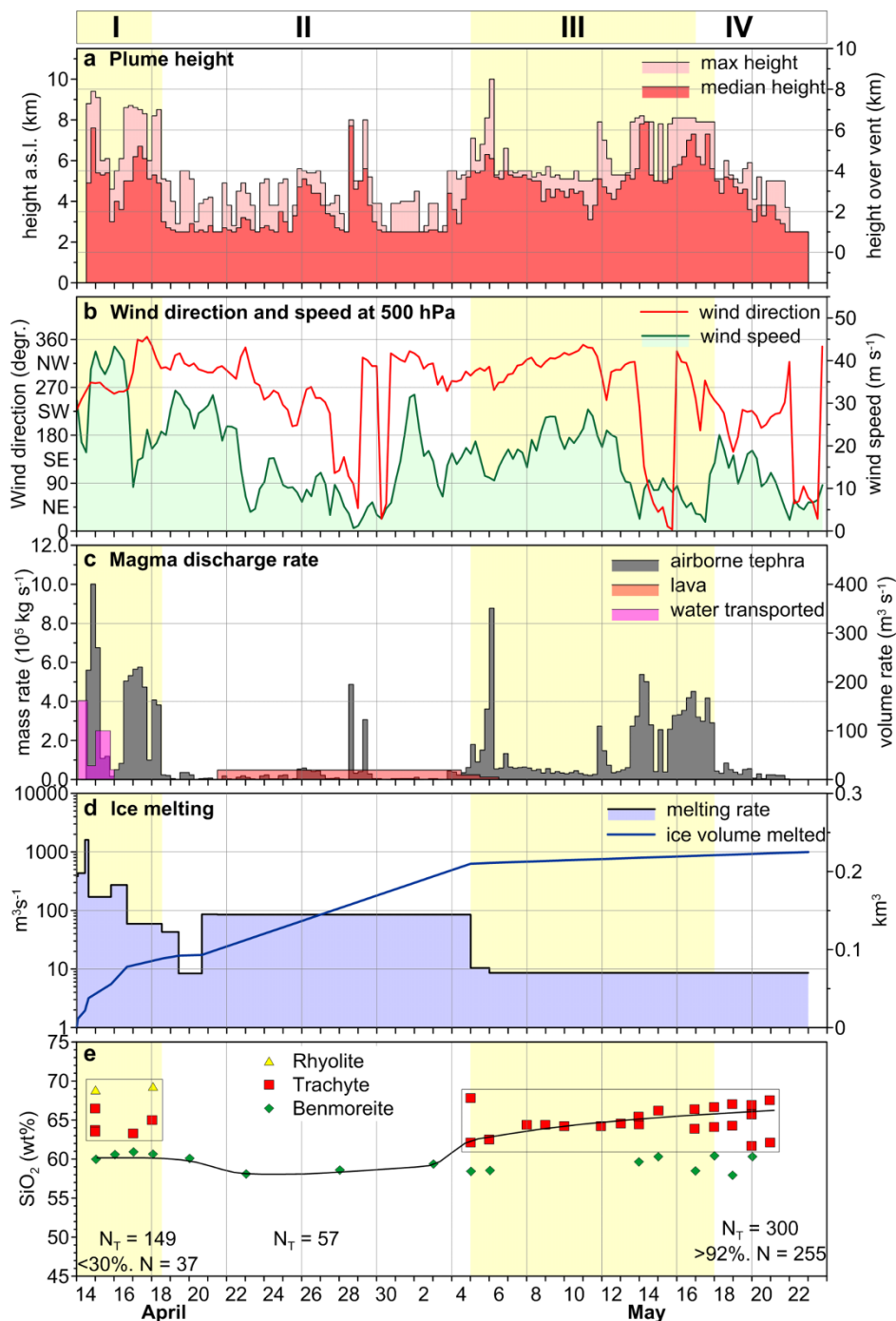


Figure 2 | Key eruption parameters. The graphs are based on tephra sampling (Figs. 3–4), plume, weather and crater observations and microprobe analyses (see Methods for details). In addition to a 3–4 hour long initial subglacial phase (not shown on graph) when the eruption melted its way to the glacier surface, the eruption is subdivided into four main phases (I–IV on graph): I: The first explosive phase, 14–18 April; II: Low-discharge mainly effusive phase, 18 April–4 May; III: Second explosive phase, 5–17 May; IV: Declining phase, 18–22 May. (a) Six hourly mean and maximum values of plume altitude based on weather radar in Keflavík (155 km west of the volcano); (b) Wind speed and direction at the 500 hPa level (approximately 5 km) over Eyjafjallajökull April 14–May 23 (see Methods); (c) Magma discharge during the eruption based on combining plume and tephra dispersal data (see Methods for details). (d) Cumulative volume of ice melted in the eruption based on changes in ice cauldrons and ice surface elevation. (e) SiO₂ content of groundmass glass (= melt) in tephra grains from individual days with 3–37 grains behind each data point (one standard deviation equal to symbol size). The groundmass glass falls into distinctive compositional groups, designated as benmoreite, trachyte and rhyolite. The relative abundance of more evolved groundmass glass compositions (highlighted) in the initial and second explosive phases is given by the percentage above the black squares. Shifts in the melt composition are in phase with shifts in magma discharge and style of activity.

a 5–10 km high plume that alternated between shades of white (steam-rich) and dark grey (loaded with ash). In the first two days, the eruption formed ice cauldrons¹¹ over the vents (Fig. 1a and 1b). The main activity on 14 April was in

the south ice cauldron, but moved to the west cauldron on 15 April where it remained until the end of the eruption (Fig. 1b). Ice melting caused repeated jökulhlaups (glacial outburst floods) on 14–15 April. Part of the erupted material

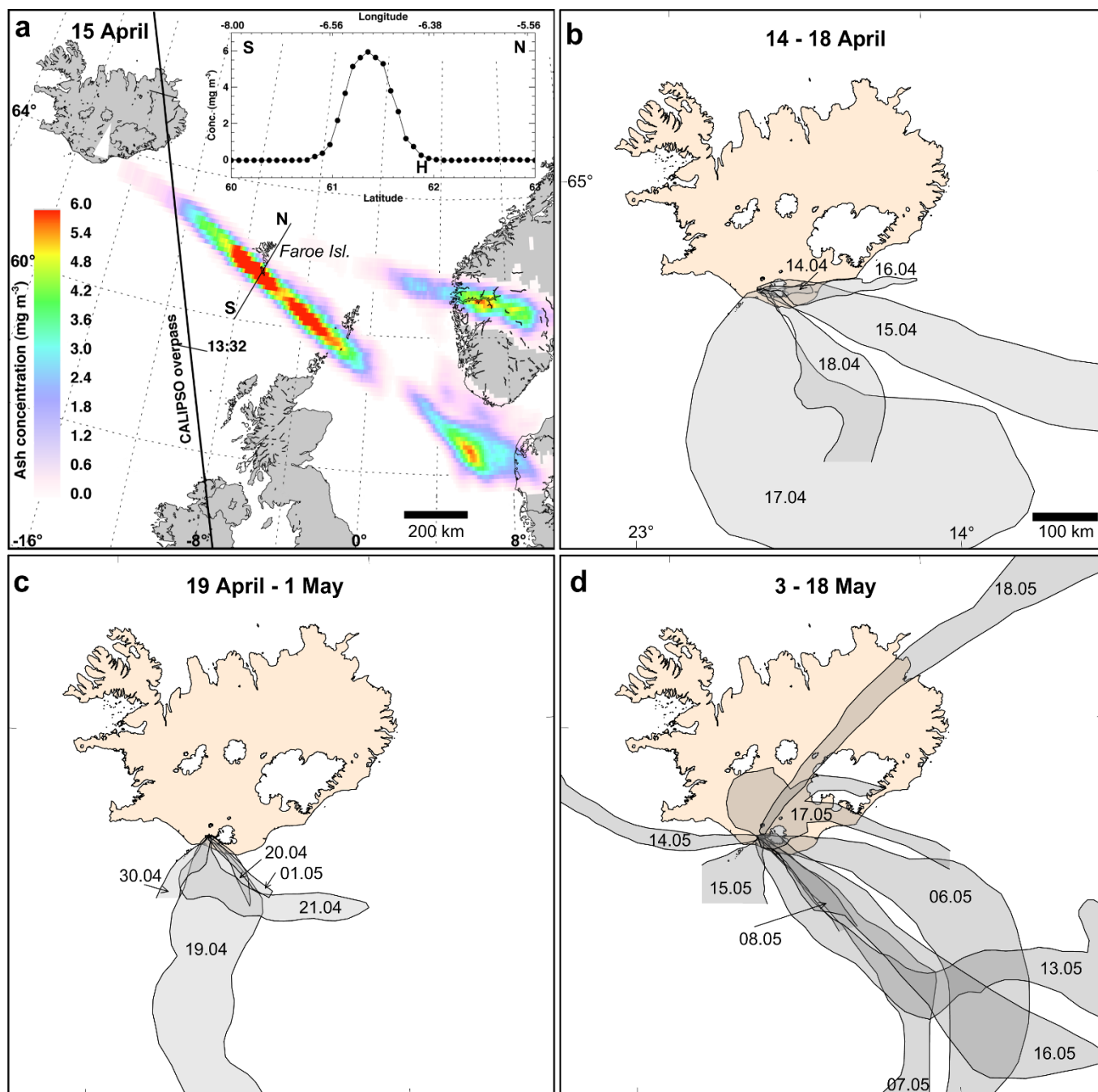


Figure 3 | Ash concentration and distribution from satellite data. (a) Ash concentrations in a vertical column for 15 April from SEVIRI retrievals. The inset shows the concentration on a section S-N over the Faroe Islands. On the graph H marks the position of the sampling locality at Hoyvik. (b–d) Distribution patterns of the tephra over Iceland and in its vicinity, based on satellite images from MODIS, MERIS and NOAA AVHRR. One image is used per day but data for some days are missing, usually because of unfavorable cloud cover. The sectors identified for each image denote the area over which ash can be detected on the images and no distinction is made between dense and highly diluted clouds.

was water-transported pyroclasts, essentially identical to the air transported tephra. This phase is conveniently divided into 14–16 April when the tephra formed a well-defined sector towards the east, and 17- to early 18 April, when northerly winds carried the tephra southwards (Figs. 3–4 and 6, Table 1). The composition of the erupted melt is predominantly evolved benmoreite (Fig. 2e). Airborne ash was detected over $1.5\text{--}2 \cdot 10^6$ km² (Fig. 4).

II. *Low-discharge effusive phase (18 April–4 May)*. During this period the melt composition was slightly less silicic, with the SiO₂ content reduced from 60–61 wt% to 58–59 wt% (Fig. 2e)

and the magma discharge dropped to $0.5\text{--}9 \cdot 10^4$ kg s⁻¹ ($\approx 2\text{--}35$ m³ s⁻¹ DRE). The activity was typified by lava effusion as a 3 km long lava flow made its way northwards out of the caldera down the outlet glacier Gigjökull (Fig. 1). Explosive activity was relatively weak but sustained, producing 2–4 km high plumes. Satellite-detected ash spread out over $0.1\text{--}0.2 \cdot 10^6$ km² (Fig. 4).

III. *Second explosive phase (5–17 May)*. The onset of this phase is marked by abrupt rejuvenation of explosive activity that coincides with sudden change in melt composition from benmoreite to trachyte (Fig. 2e). The magma output was

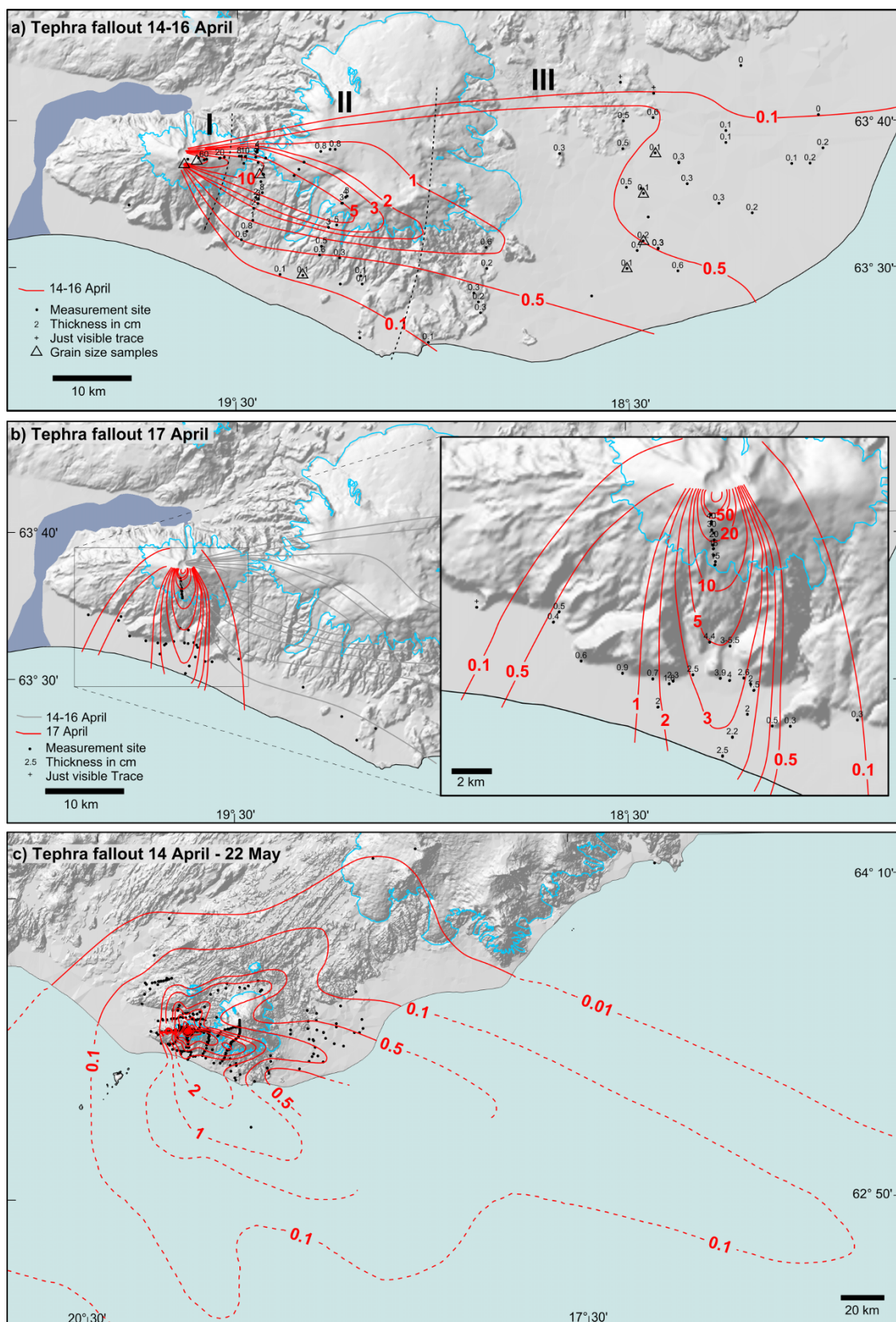


Figure 4 | Isopach maps (thickness in cm) of tephra distribution during Phase I (the first explosive phase) 14–18 April and the whole eruption (c). (a) Deposition on land during the 14–16 April, the first three days of the first explosive phase, erupting from a water-filled vent. The nine localities where grain size analysis was carried out and the three zones on land (I–III) used to estimate the grainsize distribution for 14–16 April are shown. The most intense fallout occurred from 18:30 on 14 April into the early hours of 15 April. (b) Deposition on land during the second part of the first explosive phase (17 April until early 18 April). A 6–7 km high, two-tiered tephra-laden plume typified the activity on 17 April, causing total darkness for 20 hours in the Eyjafjöll district south the volcano. (c) Total fallout on land in the eruption (14 April–22 May) and estimated fallout thickness (dotted lines) to the south and southeast of Iceland (see Methods and Figs. 5 and 6).

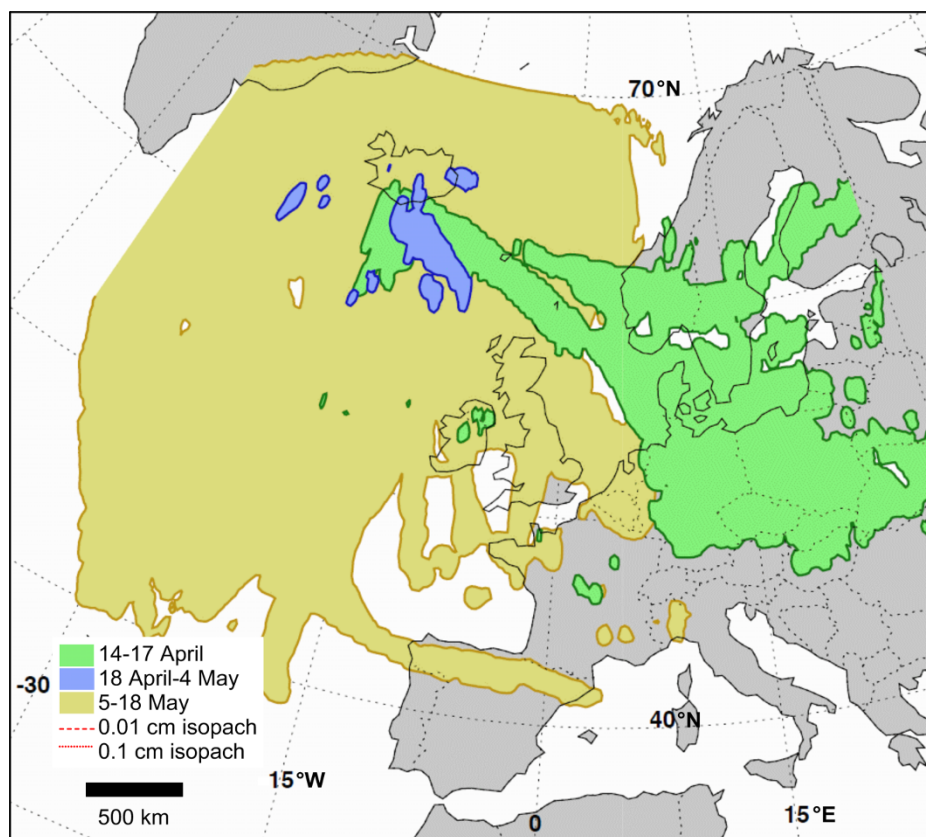


Figure 5 | Airborne ash detected outside Iceland within 40°–70°N and 40°W–30°E. The map is constructed by dividing SEVIRI retrievals into three separate time intervals: 14–17 April, 18 April–4 May and 5–18 May. Daily ash mass loadings that exceed 0.2 g m^{-2} within each $0.25^\circ \times 0.25^\circ$ grid cell are summed up. No attempt is made to indicate the amount of ash retrieved or the concentration, rather the plot shows the spatial distribution of the ash over the domain considered.

variable, shifting between periods of relatively low ($0.3\text{--}0.8 \cdot 10^5 \text{ kg s}^{-1} \approx 15\text{--}30 \text{ m}^3 \text{ s}^{-1}$ DRE) and high ($2.5\text{--}9 \cdot 10^5 \text{ kg s}^{-1} \approx 100\text{--}350 \text{ m}^3 \text{ s}^{-1}$ DRE) discharge (Fig. 2c). The average ice melting rate in the vent area was $\sim 10 \text{ m}^3 \text{ s}^{-1}$ (10^4 kg s^{-1}), confirming thermal energy loss from magma to ice. Variable wind directions coupled with a duration of 13 days resulted in considerably wider dispersal than in the first explosive phase, with ash being detected over an area of $>5 \cdot 10^6 \text{ km}^2$ (Fig. 4).

- IV. *Final phase (18–22 May)*, the period when the eruption declined and eventually continuous activity stopped. Explosions occurred on 4–8 June, but these involved minute amounts of magma, and caused limited dispersion of tephra, confined to an area within 1 km of the vents. A steam plume from the summit crater persisted for months after the eruption.

On the basis of the magma petrology and its evolution with time¹² and the deformation and seismicity before and during the eruption⁸, the course of events has been explained by injection of basaltic magma from the mantle and its mixing and mingling with pre-existing silicic magma residing in the crust under the volcano¹². Repeated peaks in activity observed during the second explosive phase (Phase III, 5–17 May, see Fig. 2c) were preceded by deep earthquakes explained by injection of new basaltic magma^{8,12}. The lack of injection of new basalt in late May is considered to have stopped the eruption, not the exhaustion of silicic magma in the crust¹².

Tephra fallout and distribution. Although the tephra fallout was most prominent in the sectors to the south and east, the prolonged explosive activity resulted in full 360° dispersal around the volcano forming a continuous tephra blanket extending from 30 up to 80 km

distance from the source vents (Fig. 4). On 14–16 April ash was carried eastward by westerly upper-tropospheric winds, while on 17 April northerly winds directed the plume to the south (Fig. 4a and 4b). Ash clouds were reported in Northern and Western Europe in the period 15–21 April and again between 6 and 17 May^{6,7}. The strong northwesterly flow persisted until 24 April, when it was replaced by weaker westerly flow (Fig. 2b). In early May, when the vigour of the eruption again intensified, the atmospheric flow turned northwesterly and remained through the latter half of May although the strength of the air flow gradually weakened. The eruption plume was directed east- or southwards for 28 out of 39 days of sustained activity. The weather situation during the spring of 2010 was indeed rather unusual with frequent northwesterly winds and a large deviation from the climatological mean atmospheric circulation¹³. The persistent northwesterly winds contributed strongly to the dispersal of ash clouds to Europe.

The maximum thickness of the tephra fallout exceeds 30 meters in the cone ramparts lining the rims of the ice cauldrons, falling abruptly to 1 m over a distance of 2 km from the source vents. With the exception of the northwest peninsula (the region of Vestfirðir), dusting of ash was reported in most parts of Iceland. The total amount of airborne tephra produced in the eruption is $270 \pm 70 \cdot 10^6 \text{ m}^3$ (bulk volume, density 1400 kg m^{-3}) of which $140 \pm 20 \cdot 10^6 \text{ m}^3$ fell in Iceland. This value is obtained by combining isopach map integration on land with integrating a piecewise exponential model of decline of thickness with distance for the area south of Iceland (see Methods). The volume of $130 \pm 50 \cdot 10^6 \text{ m}^3$ outside Iceland is based on the form of the exponential segments using the estimate for the fallout south of the Faroe Islands (see Methods) as one point of data and the reported minor fallout in various parts of

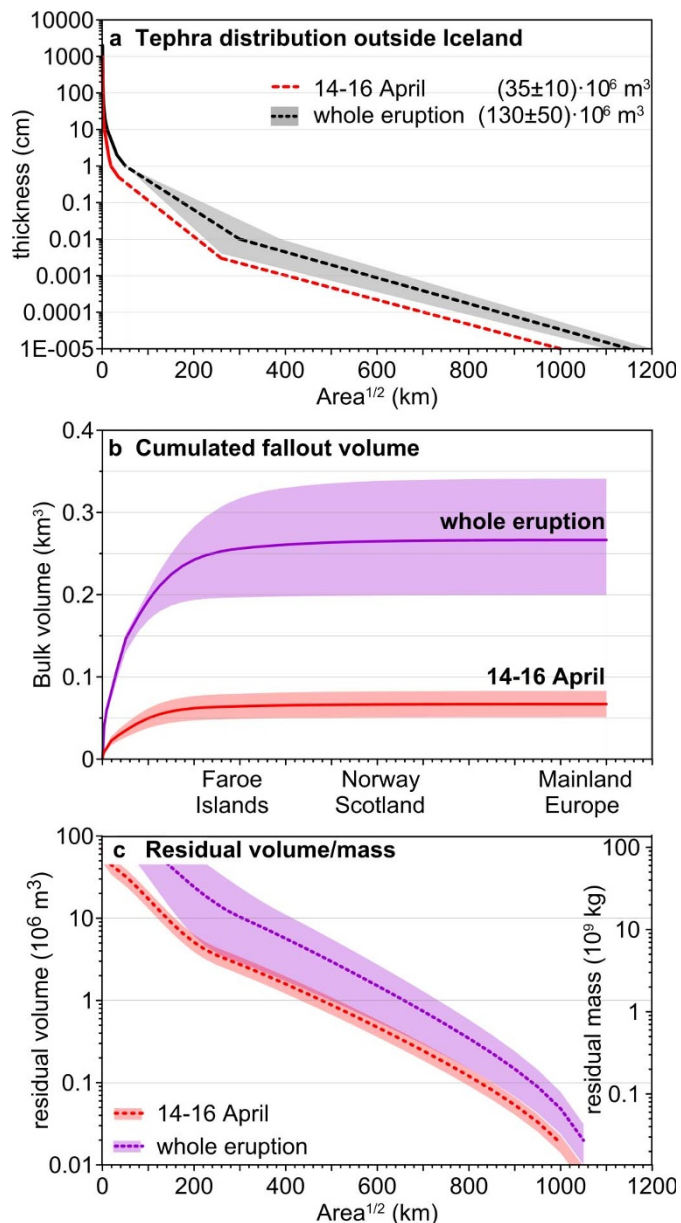


Figure 6 | Estimates of distribution outside Iceland and the volume of tephra erupted. The tephra from 14–16 April is estimated separately since it forms a well defined sector and was responsible for the first ash transported to Europe. (a) Tephra thickness as a function of square root of area within each isopach, using fallout in the Faroe Islands, satellite data and the established first order behaviour of tephra thicknesses declining exponentially with distance from source^{3,37,38}. (b) Estimated cumulated bulk volume of fallout volume and its distribution with distance. The volume within Iceland is found by direct integration of the onland part of the maps in Fig. 4. The volume outside Iceland is found by integrating the exponential curves (e.g. ref. 37). (c) Estimate of volume (left axis) and mass (right axis) that was transported beyond a specified area. The volume is found by integrating the exponential curves for 14–16 April and the whole eruption from the point on the square root of area axis on (a) out to infinity, using eqs. 13 and 14 in ref. (35). Values outside $A^{1/2} = 300$ km are rough order of magnitude estimates.

northern Europe as a justification of extending the exponential curve for thickness equal to $0.1 \mu\text{m}$ (a very minor dusting) out to $A^{1/2} = 1000$ km for 14–16 April and 1200 km for the whole eruption. However, it is important to note that the detailed shape of the curves beyond $A^{1/2}$ of 250–300 km is has relatively little influence, this distal

part for the whole eruption on Fig. 6a yields about 10^7 m^3 to the total estimated volume beyond the coast of Iceland, or about 8%. A further $30 \pm 10 \cdot 10^6 \text{ m}^3$ of tephra were transported out of the craters with meltwater and $23 \pm 5 \cdot 10^6 \text{ m}^3$ (bulk density 2400 kg m^{-3}) were emplaced as lava. When taking into account the water transported tephra and the lava flow, the total mass erupted is $4.8 \pm 1.2 \cdot 10^{11} \text{ kg}$, or $0.18 \pm 0.05 \text{ km}^3$ DRE (using $\rho_{\text{DRE}} = 2600 \text{ kg m}^{-3}$). The partitioning of the erupted material with total volumes and mass are given in Table 1. Estimates of production rates of tephra for each day of the eruption, main direction of dispersal (estimated from ground observations and satellite images) and grain size characteristics, when available, are given in Table 2.

Out of the $130 \pm 50 \cdot 10^6 \text{ m}^3$ of ash dispersed and deposited beyond the shores of Iceland $35 \pm 10 \cdot 10^6 \text{ m}^3$ were emitted on 14–16 April, $18 \pm 6 \cdot 10^6 \text{ m}^3$ on 17–18 April, $10 \pm 7 \cdot 10^6 \text{ m}^3$ on 18 April–4 May, $65 \pm 25 \cdot 10^6 \text{ m}^3$ on 5–17 May and finally $2 \pm 1 \cdot 10^6 \text{ m}^3$ in the final declining phase on 18–22 May (Table 1).

The 14–16 April tephra fall sector is well constrained. By integrating the model of piecewise exponential decline in tephra thickness with distance (Fig. 4) from $A^{1/2} = 260$ km (corresponding to the Faroe Islands) out to infinity, and converting the volume to mass using bulk density of 1400 kg m^{-3} the result is that the mass of ash transported beyond the Faroe Islands on 14–16 April amounted to $m = 2\text{--}6 \cdot 10^9 \text{ kg}$ (2–6 Tg). The satellite data (Fig. 3a) indicate that the cloud southwest of the Faroe Islands on 15 April was 80–100 km wide and about 1 km thick. The upper tropospheric wind speed (u) at 5–7 km elevation for 15 April was 20 m s^{-1} . Combining these data, assuming that the transport took place over time $\Delta t \approx 24$ hours, with plume width being w and z the plume thickness, we estimate the average mass concentration (c) of ash in the cloud from

$$c = \frac{m}{wzu\Delta t} \quad (1)$$

The result is an average concentration of ash in the cloud of $10\text{--}35 \text{ mg m}^{-3}$. By the time this same cloud reached Norway (1300 km from vent, $A^{1/2} \approx 600$ km), it had split into two, with each part having width of about 200 km (Fig. 5). Ash transported beyond that distance was of order $0.5\text{--}1 \cdot 10^9 \text{ kg}$ (= 0.5–1 Tg) (Fig. 6c). Using wind speed of 18 m s^{-1} the mean ash concentration obtained is of order 1 mg m^{-3} .

During 5–17 May, ash transport in any single phase probably never reached the intensity of 14–16 April. An estimate of the mass transported beyond ~ 650 km from source ($A^{1/2} \approx 250$ km) over the whole eruption is obtained by integrating the exponential thickness curve (Fig. 6a), as done above for 14–16 April, and converting to mass. The result is $4\text{--}40 \cdot 10^9 \text{ kg}$ (= 4–40 Tg). Finally, integration beyond $A^{1/2} \approx 1000$ km (Fig. 5c) and converting to mass as before suggests that the amount of ash reaching mainland Europe was most likely less than $1 \cdot 10^8 \text{ kg}$ (<0.1 Tg).

About 85% of the total airborne tephra was produced during the two explosive phases (Table 1, Fig. 2). On the basis of analysis from eight sampling localities (Fig. 4a, and ref. 14) the main characteristics of the deposit from 14–16 April have been studied (Fig. 7). By partitioning the sector into four zones on the basis of distance from vent (Zone I: 0–6 km, Zone II: 6–30 km, Zone III: 30– ~ 80 km, with Zone IV including all fallout outside the coast) grain sizes for each sector have been estimated and combined into a whole deposit estimate. No grain size analyses exist for the offshore part (Zone IV) so we use the Zone III data there also. The results indicate that 94% of tephra erupted on 14–16 April was finer than $1000 \mu\text{m}$, and 48–50% was ash finer than $63 \mu\text{m}$. Furthermore, $\sim 35\%$ of the total was finer than $30 \mu\text{m}$, which is probably an underestimate since it is expected that the finest ash was carried further and preferably deposited beyond the coast. This is supported by modal and maximum grain sizes observed in the Faroe Islands (mean = $40 \mu\text{m}$; max $\sim 100 \mu\text{m}$), Norway (mean = $48 \mu\text{m}$; max $\sim 90 \mu\text{m}$), the British Isles



Table 1 | Results on tephra and lava erupted at Eyjafjallajökull, April 14–May 22, 2010. In converting volumes to mass the density of tephra is taken as 1400 kg m⁻³, and that of lava 2400 kg m⁻³ (See Methods for details)

Period	All airborne tephra	Tephra fallen in Iceland	Tephra outside Iceland	Tephra water transp	Lava (21.4.–3.5.)	Mass total
Phase no. and dates	10 ⁶ m ³	10 ⁶ m ³	10 ⁶ m ³	10 ⁶ m ³	10 ⁶ m ³	10 ¹¹ kg
Phase I - east: 14–16.4	70±15	35±5	35±10	25±5	0	1.3±0.3
Phase I - south: 17–18.4	25±7	7±1	18±6	0	0	0.4±0.1
Phase I - total: 14–18.4	95±22	42±6	53±16	25±5	0	1.7±0.4
Phase II: 18.4–4.5	30±10	20±3	10±7	5±1	23±5	1.1±0.3
Phase III: 5–17.5	135±35	70±9	65±26	0	0	1.9±0.5
Phase IV: 18–22.5	10±3	8±2	2±1	0	0	0.1±0.03
Total	270±70	140±20	130±50	30±6	23±5	4.8±1.2

(mean = 25 µm; max ~100 µm), and Hungary (mean = 2–4 µm; max ~6 µm)¹⁵. Furthermore, ash aggregates ranging from 60–200 µm (mean = 85 µm) in diameter fell in the UK¹⁵. Other observations from mainland Europe indicate particle sizes up to 20 µm⁶. Considering that the total mass of airborne tephra erupted in 14–16 April was (1.0±0.2)·10¹¹ kg (equal to volume of 70±15·10⁶ m³ using bulk density of 1400 kg m⁻³). This puts the mass of <30 µm particles in this phase alone at (3.5±1.2)·10¹⁰ kg (35±12 Tg).

Comparable whole deposit grain size analyses have not yet been completed for later phases of the eruption. However, both field observations in the region within 10 km from the vents in the summers of 2010 and 2011 and individual grain size analyses (Table 2) indicate that during phase II (18 April–4 May) the tephra produced was coarser (Table 2) with the percentage of very fine ash much reduced. During high magma discharge in Phase III (5–17 May), tephra was sampled in a systematic manner with a number of traps around the volcano. In Table 2, results of grain size analysis of samples from traps located on the dispersion axis or very close to it are included. These results do not substitute for whole deposit grain size analyses but indicate that about 35–50% of the ash that was sampled from the most powerful/intense explosive phases at distance of 10–15 km from the vents was finer than 63 µm and 10–30% was finer than 30 µm (Table 2). This is slightly lower, but comparable to that of the initial phase of the eruption.

The clast populations (Fig. 5) in the first and second explosive phases (Phases I and III) are predominantly angular¹⁶, indicating brittle fragmentation of the magma^{17,18}. The grains are typically poorly to non-vesicular (<30% vesicles) with moderate to high abundances (30–90 modal %) of microlites and their groundmass glass is outgassed¹⁹. Analyses of grain morphology for the different phases indicate that phreatomagmatic activity was influential in the first explosive phase, evidence of both magmatic and phreatomagmatic fragmentation were found during the second weak phase, while in the third, explosive phase, magmatic fragmentation had become dominant²⁰. Dellino et al.²⁰ suggest that stress-induced reaction of microvesicular, fragile melt was responsible for the fragmentation once water access to the vents was exhausted.

Discussion

The eruption plume never exceeded 10 km in elevation (Fig. 2a) and classifies as weak¹, having a 0–1 km high gas thrust region with the wind diverting the buoyant plume above this elevation. The prolonged duration (Fig. 2) contrasts with Plinian eruptions that usually last for some hours rather than days^{2,21}. Moreover, the 2010 eruption demonstrates that despite its moderate size, atmospheric loading at upper tropospheric levels (4–9 km) can be substantial and widespread exceeding areas well over 10⁶ km². It is likely that the high proportion of fine-grained ash was of major importance, allowing a fraction of the fine ash to disperse widely. The settling time in the atmosphere of <60 µm particles, initially at 5–10 km elevation, is of the order of a few days^{22,23}, or significantly longer than the travel time

between Iceland and Northern Europe. However, the abundance of very fine ash beds (often loaded with ash aggregates) on land in Iceland testifies to the importance of aggregation in explaining the heavy fallout observed in the proximity of source vents^{24–26}. At larger distances, sedimentation of the very fine ash was much slower within the widespread diluted ash clouds over Europe (Fig. 5) as was observed in the days following the eastwards directed plume of 14–16 April¹⁶. However, aggregation is also important during sedimentation in the far-field regions as clearly indicated by the observations in the UK¹⁵. It should be noted that the synoptic meteorology also influences the ash sedimentation rate, as indicated by lidar observations in the UK and Germany showing the ash cloud to be a sloping structure and parallel to a weather front²⁷.

Application of satellite data to infer mass loading of the atmosphere during volcanic eruptions holds great potential in enhancing aviation safety and successful routing of aircraft in the vicinity of ash clouds. Stohl et al.⁷ estimated the total amount of ash finer than 28 µm in diameter in the Eyjafjallajökull eruption as 8.7±4.2 Tg. Our grain size data are confined to land and at present only allow a full grain size distribution estimate for 14–16 April, indicating 33±12 Tg of <28 µm for that phase alone. This leaves out substantial fallout of <28 µm particles on 17 April and in the second explosive phase on 5–17 May (Table 2), during which it may have been 10–20% of the erupted tephra. Thus, the 14–16 April estimate is in all likelihood accounting for less than half of the total of the <28 µm fraction generated in the eruption. Thus, the true value of <28 µm ash erupted in all phases combined is estimated to have been at least 70 Tg, one order of magnitude higher than the published estimates based on satellite retrievals^{6,7}. A likely reason for such a discrepancy might be that satellite retrievals for mass concentration do not work in dense, optically opaque eruptions clouds²⁸, and may therefore not provide reliable estimates close to a volcano where aggregation-enhanced settling can be a major factor.

Although only partial information on grain sizes exists at present, it is instructive to compare the Eyjafjallajökull eruption with other eruptions. It holds for the first explosive phase that the proportion of fine ash (<1000 µm) is comparable to that of the VEI 4–5 eruptions of Mount St. Helens in 1980 (dacite), El Chichon in 1982 (trachyandesite)²³ and the phreatoplinian C phase of the Askja eruption in 1875 (rhyolite)²⁹, and considerably larger than in e.g. the VEI 3 andesitic eruption of Mount Spurr in Alaska in 1992 (ref. 23). For the very fine ash (<30 µm) the proportion in Eyjafjallajökull was significantly less than in El Chichon and Mount St. Helens where elutriation of ash derived from pyroclastic flows may be partly responsible for the large percentage of very fine ash²³. Pyroclastic flows were largely absent at Eyjafjallajökull and the high percentage of fines must be due to fragmentation within the conduit, including both external water access (in the first explosive phase) and the rheological properties of the magma²⁰. The Eyjafjallajökull eruption clearly demonstrates that very high degrees of fragmentation can occur in relatively modest eruptions.



Table 2 | Approximate estimate of airborne tephra produced per day 14 April–22 May and main tephra dispersion directions. $\Delta M/\Delta t$ is estimated tephra mass erupted per day, based on partitioning of tephra erupted using the scaled version of the Mastin et al. equation (see Methods). The three columns on the right give grain size data where it is available: distance from vent where grain size samples were taken and the proportion of particles $<63 \mu\text{m}$ ($\phi > 4$) and $<31 \mu\text{m}$ ($\phi > 5$). Same information is given at other dates for representative samples. The first nine grain size samples are from the tephra deposited during the period 14–16 April, including data from Gíslason et al.¹⁴

Date	$\Delta M/\Delta t$ 10 ⁹ kg/day	Direction of dispersal	Grain size sample distance km	Grain size % <63 μm	Grain size % <31 μm
14 Apr	40–50	E	1	21	11
			2	24	15
			10	13	11
			10	17	11
15 Apr	5–10	E	58	44	33
			60	56	45
			58	70	51
			56	65	45
16 Apr	30–40	E	21	26	17
17 Apr	30–40	S	11	47	33
18 Apr	5–10	SE	-	-	-
19 Apr	1–3	SE	-	-	-
20 Apr	<1	SE	-	-	-
21 Apr	<1	SE	-	-	-
22 Apr	<1	SE	4	7	4
23 Apr	1–2	E	-	-	-
24 Apr	1–2	E	-	-	-
25 Apr	2–3	NE	-	-	-
26 Apr	3–5	E	-	-	-
27 Apr	<1	N	-	-	-
28 Apr	10–15	W	-	-	-
29 Apr	5–10	SE	-	-	-
30 Apr	<1	N	-	-	-
1 May	<1	SE	-	-	-
2 May	<1	SE	-	-	-
3 May	1–2	E	-	-	-
4 May	5–10	E	-	-	-
5 May	30–40	SE	30	46	29
6 May	5–10	E	-	-	-
7 May	5–10	SE	-	-	-
8 May	3–5	SE	13	12	10
9 May	2–5	SE	-	-	-
10 May	2–5	SE	13	12	10
11 May	10–20	SE	-	-	-
12 May	3–5	E	-	-	-
13 May	20–30	SE	10,13	38	23
14 May	20–30	W	14	10	8
15 May	15–25	SW	-	-	-
16 May	30–40	SE	-	-	-
17 May	20–30	E	-	-	-
18 May	3–5	NE	-	-	-
19 May	3–5	NE	8	42	27
20 May	1–3	NE	-	-	-
21 May	<1	E	-	-	-
22 May	<1	W	-	-	-

The 2010 eruption at Eyjafjallajökull acutely demonstrated that a moderate size explosive eruption can produce widely dispersed volcanic plumes and cause major disruptions to air travel. In Europe, a number of Italian volcanoes have and will in the future produce intermediate to silicic explosive eruptions with large amounts of fine ash. However, in terms of eruption frequency and potential for disruption, Icelandic volcanoes are the most potent^{30,31}. Upper tropospheric winds are usually most influential in determining the direction of dispersal of tephra from Icelandic eruptions, tending to have a component of eastbound flow, with northwesterly winds slightly less common than southwesterlies³¹. Quantitative analysis of the probabilities for magnitude and duration of explosive eruptions in Iceland is beyond the scope of this study. However, the existing records show that about 10–15 eruptions with a volcanic explosivity

index VEI = 3 (ejecta volume 0.01–0.1 km³) or larger occur in Iceland every century³², and between 1970 and 2010 seven such eruptions occurred with tephra generation lasting from about an hour to 1.5 days^{33,34}. Southwesterly upper tropospheric winds were dominant during these events carrying tephra towards northeast. Hence, only minor disruption to air traffic occurred and the busy air routes in central and western Europe were not affected. Finally, basaltic phreatomagmatic eruptions in Iceland such as some of those from Katla, the larger and neighbouring volcano to Eyjafjallajökull^{35,36} typically last several days or even weeks. Such eruptions may have higher ash discharge than observed at Eyjafjallajökull. The most recent explosive eruption in Iceland, the one at Grímsvötn in May 21–28, 2011, was basaltic and of greater intensity than the 2010 Eyjafjallajökull eruption, as indicated by its 15–20 km high eruption

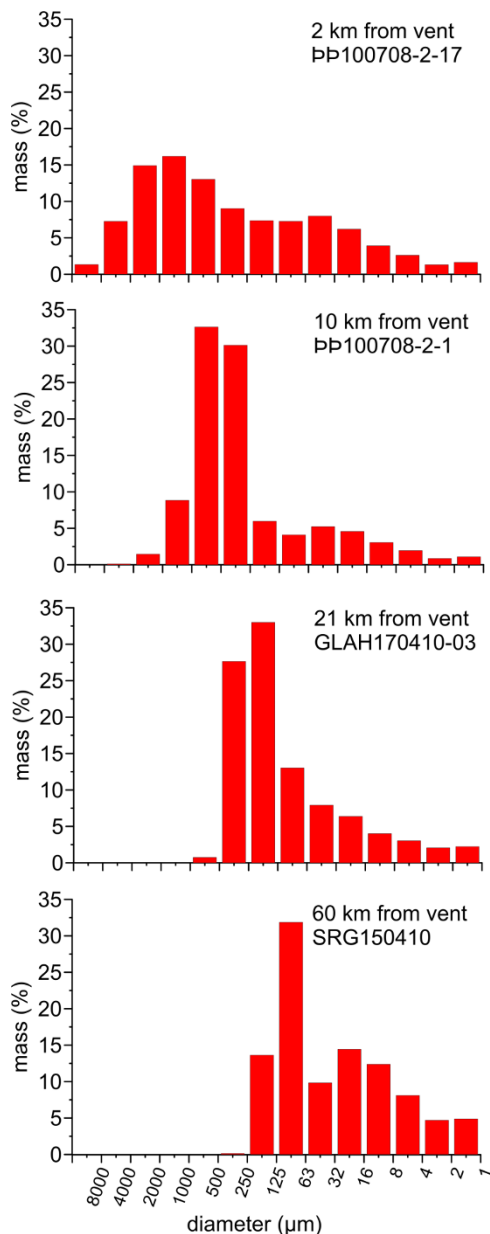


Figure 7 | Grain size distributions for 14–16 April. Results for samples from four different localities within the on-land part of the 14–16 April eastwards directed tephra sector of Phase I at distances of 2, 10, 21 and 60 km (see Fig. 4a for location).

column. Preliminary results from mapping the Grímsvötn 2011 fall deposits also indicate two to three times larger bulk volume of erupted tephra compared with Eyjafjallajökull 2010 (Institute of Earth Sciences, Univ. Iceland, unpublished data). Distal fallout was observed in at least the British Isles and Norway (University of Edinburgh, unpublished data), yet disruption to air traffic was minor compared to the previous year, despite higher eruption rates and total volume. The relatively short duration and absence of strong upper tropospheric and stratospheric winds prevented dispersal at the scale observed in April–May 2010. This illustrates the complicated nature of the hazard caused by ash dispersal from volcanic eruptions.

Methods

Our results are based on measurements of tephra thickness on land in Iceland, records of tephra fallout outside Iceland, reconstruction of plume dispersal from satellite images, monitoring and mapping of ice melting, eruption plume height, grain size analysis of tephra, tephra grain morphology and chemistry of the erupted products.

Vent development and ice melting. Monitoring of vents and ice cauldron formation (Figs. 1, 2) was done using the Icelandic Coast Guard Dash 9 aircraft, equipped with a Synthetic Aperture Radar (SAR)¹¹. Ice melting rates were estimated from (1) growth of ice cauldrons as measured from the SAR images, (2) evolution of crevasse patterns and other subsidence structures around the ice cauldrons from photographs and the SAR images, and (3) mapping of ice surface with GPS in July 2010.

Tephra volume in Iceland. The tephra on land consisted of airfall (dominant), and water transported (minor). For the airfall tephra thicknesses were measured in about 400 locations and used to construct the isopach maps. Tephra volume within the mapped area was found by directly integrating the isopach maps. Volume outside the 0.01 cm contour on land (approximately $2 \cdot 10^6 \text{ m}^3$) was estimated using exponential decline in thickness with distance^{37–39}. In addition, the material left within the two main ice cauldrons at the end of the eruption was estimated from the difference between the depth of the partly tephra-filled cauldrons and the depth to pre-eruption bedrock ($\sim 33 \cdot 10^6 \text{ m}^3$). Error estimates for isopach maps on land are considered to be 15%. Separate isopach maps were constructed for the east-directed sector formed on 14–16 April, the south-directed sector formed on 17 April and for the whole deposit (Fig. 4). The volume of tephra deposited on land for the period 18 April–22 May was obtained by subtracting the volume erupted on 14–18 April from the whole-deposit map. The partitioning between 18 April–4 May, 5–17 May and 18–22 May is estimated from (1) the integrated plume height over the two periods (eq. 2, see below), and (2) relative thickness of deposits for the two periods on Eyjafjallajökull based on our measurements in July 2010 and August 2011.

Tephra volume outside Iceland. We assume piecewise exponential decline with distance^{37–39}. The magnitude is constrained from distribution of ash as observed from satellite images showing eruption cloud distribution pattern analysis of MODIS, MERIS and NOAA AVHRR satellite images (Figs. 3 and 4). Very fine ash fell in Hoyvik in the Faroe Islands (about 1 g/m^2 , ref. 40) at the northern margin of the main plume of April 15–16. We assume that fallout was proportional to estimates of the satellite retrievals of volcanic ash mass loadings (see below) and in that way derive a rough estimate of maximum fallout south of the islands as 40 g/m^2 , corresponding a thickness of 0.03 cm. The form of the dotted contours outside the coast on Fig. 4c is based on the plume locations documented on Figs. 3b–c, while the area covered by each contour is defined in such a way that direct integration would yield the same result as the piecewise exponential model. Error estimates for material deposited outside Iceland are based on a minimum extrapolation that still allows for some material to be transported past the Faroe Islands and a maximum estimate that still limits fallout equivalent to $0.1 \mu\text{m}$ thickness ($\sim 0.14 \text{ g m}^{-2}$ – e.g. 0.5–1% of a surface would contain a particle if all particles were $10 \mu\text{m}$ in diameter) to the northern coast of mainland Europe. These estimates place the relative error at about 40%.

Conversion from tephra volume to mass is obtained by using bulk tephra density of $1400 \pm 40 \text{ kg m}^{-3}$, found by averaging the results from 14 sampling locations obtained at various times between 15 April and 20 May (range $1195\text{--}1689 \text{ kg m}^{-3}$ and standard deviation of 130 kg m^{-3}). The same value is used for water-transported tephra. Our results are essentially identical to the mean value of 1443 kg m^{-3} obtained by Bonadonna et al. for fallout from 4–8 May⁴¹. Representative samples yielding a reliable value for the lava flow are lacking but a value of 2400 kg m^{-3} is used, a reasonable value for lava that has experienced considerable water interaction (e.g. ref. 42).

Grain size analysis was done by hand sieving down to 125 or 63 μm and a Sympatec laser diffraction analyser down to 2 μm . Total grain size partitioning for the 14–16 April east-directed sector was done by defining the three zones on land (Fig. 4a) as Voronoi Tessalation (nearest neighbor) cells³⁸ using average values for the grain size samples within each zone (two in Zone I, two at the same locality in Zone II and one on the southern part of the sector, and four¹¹, all at 58–60 km distance from vent in Zone III). The values from Zone IV are used for Zone IV (offshore).

Satellite retrievals of volcanic ash mass loadings^{27,43–44} are made using measurements from infrared channels of the geosynchronous Meteorosats Second Generation (MSG) Spin-stabilized Enhanced Visible and Infra-red Imager (SEVIRI), with a temporal sampling time of 15 min. SEVIRI observes the earth disk over a total field of view of 70° in 12 channels from the visible to the infrared with a temporal sampling time of 15 min, and a spatial resolution of $\sim 10 \text{ km}^2$ at the sub-satellite point, increasing to $\sim 100 \text{ km}^2$ near the edges of the scan.

Eruption plume height (Fig. 2) was monitored with weather radar at Keflavík, 150 km to the west of the volcano, sampling every 5 minutes⁴⁵, but six hourly values of mean and maximum height are presented.

For the isopach maps on land and piecewise exponential decline outside Iceland we obtain total volume for different periods. In order to partition the erupted material into shorter periods of six hours (Fig. 2), we use the record of plume height and then apply a scaled version of the empirical formula of Mastin et al.²¹

$$Q_i = 0.0564k_i \left[\frac{H_{\text{med}} + H_{\text{max}}}{2} \right]^{4.15} \quad (2)$$

Here Q_i is average magma discharge for the 6 hour interval (in $\text{m}^3 \text{ s}^{-1}$ of magma). We convert the volume discharge into mass discharge using DRE density 2600 kg m^{-3} , applicable to magmas of intermediate composition. H_{med} and H_{max} are respectively the median and maximum values of plume height over vent for the interval. k_i is the scaling factor found by comparing the value obtained by integrating eq. (1) (with $k_i = 1$) with the actual mapped fallout over three different periods of the eruption. The



scaling factor k_i is found to take the values 2.15 for 14–16 April, 1.58 for 17 April and 1.59 for 18 April–22 May. Note that these scaling factors are dependent on our choice of using the mean of median and maximum height for each interval; slightly different scaling values are found if 5 minute plume height data is integrated directly⁴⁵. We are not attempting to refine the Mastin formula in any general way, only scale it in such a way that when integrated it yields values that fit our total volume estimates. The plume was pulsating over long periods, displaying considerable variations in height over time scales of hours. The maximum height might also be applied or the use of shorter intervals, leading to slightly different values of k_i . However, we find that the results shown in Table 1 are not significantly affected by the interval length (5 min., 3 or 6 hours) or whether maximum or mean plume height is used. The six hourly means, however, require minimal editing or interpolation of gaps in the plume height record⁴⁵ and are therefore used here. As noted above, we also use the scaled plume discharge values from equation (2) to estimate partitioning of the volume obtained for 18 April–22 May into the individual main phases (Table 1).

Wind speed and direction at approximately 5 and 7 km altitude is retrieved from the operational analysis of the European Centre for Medium Weather Forecasts (ECMWF).

Composition of the magma was obtained by Cameca SX100 electron microprobe at the University of Edinburgh⁴⁶. Scanning electron microscope (SEM) images were obtained with a Leo Supra 25 instrument.

- Wilson, L., Sparks, R. S. J., Huang, T. C. & Watkins, N. D. The control of volcanic column heights by eruption energetic and dynamics. *J. Geophys. Res.* **83**, 1829–1836 (1978).
- Sparks, R. S. J. *et al.* (eds): *Volcanic Plumes* Wiley and Sons, Chichester, 574 pp (1997).
- Thorarinsson, S. The tephra fall from Hekla on March 29th, 1947. In: *The eruption of Hekla 1947–1948*, **2**, 1–78 (1954).
- Ansmann, A. *et al.* The 16 April 2010 major volcanic ash plume over central Europe: EARLONET lidar and AERONET photometer observations at Leipzig and Munich, Germany. *Geophys. Res., Lett.* **37**, L13810 (2010).
- Pietruczuk, A. *et al.* Eyjafjallajökull volcano ash observed over Belsk (52° N, 21° E), Poland, in April 2010. *Int. J. Remote Sensing* **31**, 3981–3986 (2010).
- Schumann, U. *et al.* Airborne observations of the Eyjafjalla volcano ash cloud over Europe during air space closure in April and May 2010. *Atm. Chem. Phys.* **11**, 2245–2279 (2011).
- Stohl, A. *et al.* Determination of time- and height-resolved volcanic ash emissions and their use for quantitative ash dispersion modelling: the 2010 Eyjafjallajökull eruption. *Atmos. Chem. Phys.* **11**, 4333–4351 (2011).
- Sigmundsson, F. *et al.* Intrusion triggering of the 2010 Eyjafjallajökull eruption. *Nature* **426**, 426–430 (2010).
- Pedersen, R. & Sigmundsson, F. Temporal development of the 1999 intrusive episode in the Eyjafjallajökull volcano, Iceland. *Bull. Volc.* **68**, 373–393 (2006).
- Edwards, B. *et al.* Interactions between lava and snow/ice during the 2010 Fimmvörðuháls eruption, south-central Iceland. *J. Geophys. Res.* **117**, B04302 (2012).
- Magnússon, E. *et al.* Ice-volcano interactions during the 2010 Eyjafjallajökull eruption, as revealed by airborne imaging radar. *J. Geophys. Res.* **117**, B07405 (2012).
- Sigmarsson, O., *et al.* Remobilization of silicic intrusion by mafic magmas during the 2010 Eyjafjallajökull eruption. *Solid Earth* **2**, 271–281 (2011).
- Petersen, G. N., Björnsson, H. & Arason, P. The impact of the atmosphere on the Eyjafjallajökull 2010 eruption plume. *J. Geophys. Res.* **117**, D00U07 (2012).
- Gislason, S. R., Alfredsson, H. A., Eiríksdóttir, E. S., Hassenkam, T. & Stipp, S. L. S. Volcanic ash from the 2010 Eyjafjallajökull eruption. *Applied Geochemistry* **26**, S188–S190 (2011).
- Stevenson, J. A. *et al.* Distal deposition of tephra from the Eyjafjallajökull 2010 summit eruption. *J. Geophys. Res.* **117**, B00C10 (2012).
- Gislason, S. R. *et al.* Characterization of Eyjafjallajökull volcanic ash particles and a protocol for rapid risk assessment. *Proc. Nat. Ac. Sci.* **108**, 7307–7312 (2011).
- Papale, P. Strain-induced magma fragmentation in explosive eruptions. *Nature* **397**, 425–428 (1999).
- Büttner, R., Dellino, P., Raue, H., Sonder, I. & Zimanowski, B. Stress-induced fragmentation of magmatic melts: Theory and experiments. *J. Geophys. Res.* **111**, B08204 (2006).
- Thordarson, T. *et al.* The 14 April–22 May 2010 summit eruption at Eyjafjallajökull volcano, Iceland: Volatile contents and magma degassing. EGU General Assembly 2011. *Geophysical Research Abstracts*, Vol. **13**, EGU2011–12046 (2011).
- Dellino, P. *et al.* Ash from the Eyjafjallajökull eruption (Iceland): Fragmentation processes and aerodynamic behavior. *J. Geophys. Res.* **117**, B00C04 (2012).
- Mastin, L. G. *et al.* A multidisciplinary effort to assign realistic source parameters to models of volcanic ash-cloud transport and dispersion during eruptions. *J. Volcanol. Geoth. Res.* **186**, 10–21 (2009).
- Bonadonna, C., Ernst, G. G. J. & Sparks, R. S. J. Thickness variations and volume estimates of tephra fall deposits: the importance of particle Reynolds number. *J. Volcanol. Geotherm. Res.* **81**, 173–187 (1998).
- Rose, W. I. & Durant, A. J. Fine ash content of explosive eruptions. *J. Volcanol. Geoth. Res.* **186**, 32–39 (2009).
- Carey, S. & Sigurdsson, H. Influence of particle aggregation on deposition of distal tephra from the May 18, 1980, eruption of Mount St. Helens volcano. *J. Geophys. Res.* **87**, 7061–7072 (1982).
- Bonadonna, C. *et al.* Tephra fallout in the eruption of Soufrière Hills Volcano, Montserrat. In: Druitt T.H., Kokelaar B.P. (eds) *The eruption of Soufrière Hills Volcano, Montserrat, from 1995 to 1999. Geological Society of London, Memoir* **21**, 483–516 (2002).
- Taddeucci, J. *et al.* Aggregation-dominated ash settling from the Eyjafjallajökull volcanic cloud illuminated by field and laboratory high-speed imaging. *Geology* **39**, 891–894 (2011).
- Dacre, H. F., *et al.* Evaluating the structure and magnitude of the ash plume during the initial phase of the 2010 Eyjafjallajökull eruption using lidar observations and NAME simulations. *J. Geophys. Res.* **116**, D00U03 (2011).
- Prata, A. J. & Grant, I. F. Retrieval of microphysical and morphological properties of volcanic ash plumes from satellite data: Application to Mt. Ruapehu, New Zealand. *Quart. J. Roy. Meteorol. Soc.* **127**(576B), 2153–2179 (2001).
- Sparks, R. S. J., Wilson, L. & Sigurdsson, H. The pyroclastic deposits of the 1875 eruption of Askja, Iceland. *Phil. Trans. Roy. Soc. Lond., Series A* **299**, 241–273 (1981).
- Larsen, G. & Eiríksson, J. Holocene tephra archives and tephrochronology in Iceland - a brief overview. *Jökull* **58**, 229–250 (2008).
- Davies, S. M. *et al.* Widespread dispersal of Icelandic tephra: how does the Eyjafjallajökull eruption of 2010 compare to past Icelandic events? *J. Quat. Sci.* **25**, 605–611 (2010).
- Gudmundsson, M. T., Larsen, G., Höskuldsson, Á. & Gylfason, Á.G. Volcanic hazards in Iceland. *Jökull* **58**, 251–268 (2008).
- Thordarson, T. & Larsen, G. Volcanism in Iceland in historical time: Volcano types, eruption styles and eruptive history. *J. Geodyn.* **43**, 118–152 (2007).
- Jude-Eton, T., Thordarson, T., Gudmundsson, M. T. & Oddsson, B. Dynamics, Stratigraphy, and Proximal Dispersal of Supraglacial Tephra during the Ice-confined 2004 Eruption at Grímsvötn Volcano, Iceland based on field, observational, and tremor data. *Bull. Volcanol.* **74**, 1057–1082.
- Larsen, G. Holocene eruptions within the Katla volcanic system, south Iceland. *Jökull* **49**, 1–28 (2000).
- Elíasson, J., Larsen, G., Gudmundsson, M. T. & Sigmundsson, F. Probabilistic model for eruptions and associated flood events in the Katla caldera, Iceland. *Computational Geosciences* **10**, 179–200 (2006).
- Fierstein, J. & Nathenson, M. Another look at the calculation of fallout tephra volumes. *Bull. Volcanol.* **54**, 156–167 (1992).
- Bonadonna, C. & Houghton, B. F. Total grain-size distribution and volume of tephra-fall deposits. *Bull. Volcanol.* **67**, 441–456 (2005).
- Thordarson, T. & Höskuldsson, Á. Postglacial volcanism in Iceland. *Jökull* **58**, 197–228 (2008).
- Arting, U. & Hojgaard, B. Collecting ash samples from the Eyjafjallajökull eruption (April–May 2010) on the Faroe Islands. *Volcanological Workshop, Hvolsvöllur, Iceland*. Abstracts, 16 (2010).
- Bonadonna, C. *et al.* Tephra sedimentation during the 2010 Eyjafjallajökull eruption (Iceland) from deposit, radar, and satellite observations. *J. Geophys. Res.* **116**, B12202 (2011).
- Gudmundsson, M. T. & Milsom, J. Gravity and magnetic studies of the subglacial Grímsvötn volcano, Iceland. Implications for crustal and thermal structure. *J. Geophys. Res.* **102**, 7691–7704 (1997).
- Prata, A. J. & Prata, A. T. Eyjafjallajökull volcanic ash concentrations determined using Spin Enhanced Visible and Infrared Imager measurements. *J. Geophys. Res.* **117**, D00U23 (2012).
- Wen, S. & Rose, W. I. Retrieval of sizes and total masses of particles in volcanic clouds using AVHRR bands 4 and 5. *J. Geophys. Res.* **99**, 5421–5431 (1994).
- Arason, P., Petersen, G. N. & Björnsson, H. Observations of the altitude of the volcanic plume during the eruption of Eyjafjallajökull, April–May 2010. *Earth Syst. Sci. Data* **3**, 9–17 (2011).
- Hayward, C. L. High Spatial Resolution Electron Probe Microanalysis of Tephra and Melt Inclusions without beam-induced chemical modification. *The Holocene* **22**, 119–125 (2012).

Acknowledgements

We are extremely grateful for the contributions made by the following individuals, who at various times assisted us in the field or the laboratory: T. Ágústsdóttir, S. Gudmundsson, M. Hafnadóttir, M. Hensch, H. Jensdóttir, B.V. Óskarsson, G.M. Sigurdardóttir, J. Gudnason, M. E. Hartley, R. M. Meara, J. Gilbert, B. F. Houghton, R. Carey and S. T. Barningham. S. von Löwis, Þ. Arason and B. Palmason at the IMO were instrumental in operating the weather radar generating the time series of plume top altitudes. The Icelandic Coast Guard provided essential expertise and support for field work and monitoring. Finally, this work was made possible by direct funding from the Icelandic government, grant from the University of Iceland Research Fund as well as a NERC Emergency Grant (Ne/I00775x/1) to T. Thordarson. A helpful review by John Stix improved the quality of this paper.

Author contributions

Ground sampling and grainsize analyses was mainly done by ÁH, TT and GL, while GL, MTG and TH made distribution maps and did volume calculations. FJP analysed satellite



data for distant distribution while IJ and TH defined fallout patterns south and southeast of Iceland from satellite images. HB and GNP analysed data on wind patterns and, together with MTG and BO, weather radar data. Data from airborne monitoring were analysed by MTG, EM, BO and TH. CLH and TT performed chemical analyses and JAS analysed ash from the UK, Norway and the Faeroe Islands. MTG and TT wrote the manuscript with input from all team members.

Additional information

Competing financial interests: The authors declare no competing financial interests.

License: This work is licensed under a Creative Commons Attribution-NonCommercial-NoDerivative Works 3.0 Unported License. To view a copy of this license, visit <http://creativecommons.org/licenses/by-nc-nd/3.0/>

How to cite this article: Gudmundsson, M.T. *et al.* Ash generation and distribution from the April-May 2010 eruption of Eyjafjallajökull, Iceland. *Sci. Rep.* **2**, 572; DOI:10.1038/srep00572 (2012).